Soft Matter

Size of liquid metal particles influences actuation properties of a liquid crystal elastomer composite

Journal:	*Soft Matter*
Manuscript ID	SM-ART-02-2020-000278.R1
Article Type:	Paper
Date Submitted by the Author:	03-May-2020
Complete List of Authors:	Michael, Ford; Carnegie Mellon University Palaniswamy, Maduran; Carnegie Mellon University, Mechanical Engineering Ambulo, Cedric; University of Texas at Dallas Erik Jonsson School of Engineering and Computer Science, Bioengineering Ware, Taylor; The University of Texas at Dallas, Bioengineering Majidi, Carmel; Carnegie Mellon University, Mechanical Engineering

ARTICLE

Size of liquid metal particles influences actuation properties of a liquid crystal elastomer composite

Received 00th January 20xx,
Accepted 00th January 20xx

DOI: 10.1039/x0xx00000x

Michael J. Ford,[a] Maduran Palaniswamy[a], Cedric P. Ambulo[b], Taylor H. Ware[b] and Carmel Majidi*[a,c,d]

Composites of liquid crystal elastomer (LCE) that are electrically conductive have the potential to function as soft "artificial muscle" actuators that can be reversibly stimulated with electrical Joule-heating. Conductivity can be achieved by embedding the LCE with droplets of an alloy of gallium and indium that is liquid at room temperature. These soft artificial muscles are capable of >50 % reversible actuation with an applied load. The key to actuation at high loadings of liquid metal (LM) is that the droplets deform with the surrounding matrix. By controlling the size of LM droplets through simple processing techniques, we show that the actuator properties of the LM-LCE muscle can be tuned. For example, composites with smaller liquid metal particles (ca. 10 µm or less) are stiffer than those with larger liquid metal particles (ca. > 100 µm) and are capable of greater force output. However, smaller particles reduce actuation strain and composites with large particles exhibit significantly greater stroke length. Such tunability in actuation properties permits the fabrication of specialized soft artificial muscles, where processing of the composite controls actuation strain and actuation force.

1. Introduction

The actuation capabilities of natural muscle have inspired the development of soft actuators for emerging applications such as bio-inspired soft robotics and wearable computing. Natural muscle exhibits a large actuation stroke (> 40 %) at 0.1-0.35 MPa stress and can actuate at a strain rate of > 50 % s^{-1}.[1] Advancements in multifunctional material synthesis and processing will facilitate improvements of soft artificial muscles.

Current state-of-the-art artificial muscles include pneumatic/hydraulic actuators, dielectric elastomer actuators, and thermal actuators like shape memory alloys.[1–3] Each artificial muscle technology has distinct trade-offs. For example, pneumatic/hydraulic actuators exhibit high work output, modular actuation, and fast actuation rates but require auxiliary equipment like pumps. Dielectric elastomer actuators can be compliant and actuate quickly but require high voltages (typically > 1 kV). Untethered actuation at low voltages is possible for thermal actuators like shape memory alloys, but the energy efficiency of thermal actuators is low (typically << 1-2%)[3].

Another potential candidate for artificial muscles in future technologies are liquid crystal elastomers (LCEs, Fig. 1a). LCEs consist of a network of liquid crystal moieties and change shape when the liquid crystal order is disrupted (e.g., by heating through a liquid crystal phase transition). Properties like actuation stress, actuation strain, recyclability, and the transition temperature of the liquid crystalline phase can be modified by changing the molecular makeup of the liquid crystal moiety and/or the network.[4–9] LCEs are soft and compliant (modulus < 1 MPa) and can exhibit a large actuation stroke (> 400 %).[5,10] Shear extrusion of LCEs enable so-called 4D printed structures that can achieve arbitrary/complex actuation.[11–14] LCEs can also respond to various stimuli like ambient heat, light, electric fields, and Joule heating.[15]

For actuation that does not rely on ambient heating, LCEs have been synthesized/processed to respond to light, electric fields, or Joule heating.[15] Active response to light can be very fast[16,17] and demonstrably useful for many applications[18–20] but may be prohibitive in remote/inaccessible environments or in situations where ambient light might affect actuation. Alternatively, electric fields can be used to actuate LCEs. The electromechanical responsivity of LCEs is improved with the addition of carbon nanotubes; however, the rigid inclusions reduce actuation strain relative to the unfilled LCE.[21,22] Both light and electric field actuation are difficult to scale for artificial muscles with thicknesses greater than a few hundred micrometres. Joule heating has been accomplished with surface heaters and conductive fillers[23–28], which is promising for the development of untethered soft robots that use LCEs as soft actuators.[29,30]

We recently described an LCE composite that incorporated an alloy of gallium and indium that is liquid at room temperature.[31] The liquid metal (LM) is electrically conductive and forms a native oxide that permits the formation of micro- and nanodroplets by shearing or sonication.[32–35] The LM-LCE composite was compliant, deformable, and electrically and

[a] Department of Mechanical Engineering, Carnegie Mellon University, Pittsburgh, PA 15213
[b] Department of Bioengineering, University of Texas at Dallas, Richardson, TX 75080
[c] Robotics Institute, Carnegie Mellon University, Pittsburgh, PA 15213
[d] Department of Materials Science and Engineering, Carnegie Mellon University, Pittsburgh, PA 15213
Electronic Supplementary Information (ESI) available: Videos of actuation and additional mechanical and thermal characterizations included. See DOI: 10.1039/x0xx00000x

thermally conductive. Importantly, the liquid metal could deform with the surrounding matrix and therefore did not inhibit actuation capabilities. The LM-LCE composite exhibited robust joule-heated actuation with actuation strokes > 50%.[31]

However, it was unclear from our initial studies how LM synthesis and assembly may influence actuation characteristics. LM particle size can be easily tuned by simple shearing or with sonication, and the particle size can play a role in thermal/mechanical properties.[36–39] As particle size decreases, composite stiffening can occur due to surface tension at the solid-liquid interface.[39]

In this manuscript, we explore these trade-offs by synthesizing LM-LCE soft actuators, evaluating actuation capabilities, and examining the influence of LM particle size on actuation. LM particle sizes were tuned by simple shearing or sonication. Particle sizes were on the order of 100 μm, 10 μm, and 1 μm (referred to henceforth as *O*(100 μm), *O*(10 μm), and *O*(1 μm). Particle sizes were evaluated by electron microscopy and correlated with differences in the mechanical and thermomechanical properties of the composites. In general, we found that composites with smaller particles were stiffer than those with larger particles and that the stiffness played a role in actuation characteristics. At moderate loads (40-70 kPa), actuation strain was reduced from >50 % for LM-LCE composites that were composed of larger particles to < 5 % for LM-LCE composites that were composed of smaller particles. While LM-LCE composites with larger particles broke at loads of 80-90 kPa, LM-LCE composites with smaller particles could lift loads > 300 kPa. This tunability in the actuation stoke and stress presents a useful design space that can be leveraged for specific applications. Soft actuators were evaluated as artificial muscles for use in underwater applications and had actuation characteristics that were similar to natural muscle. The ability to deterministically tailor actuation properties through LM droplet processing represents an important step towards the continued development of LM-LCE composites for soft artificial muscle actuation.

2. Materials & Methods

2.1 LM-LCE composites

We adapted an established thiol-acrylate Michael addition reaction to synthesize LCEs.[40] The LCE mixture was prepared by first dissolving 12 g of 4-bis-[4-(3-acryloyloxypropypropyloxy) benzoyloxy]-2-methylbenzene (RM257, Wilshire Technologies) in 3 g of toluene in a 90 °C oven. After dissolution and cooling, 0.675 g of the tetrafunctional crosslinker, pentaerythritol tetrakis(3-mercaptopropionate) (PETMP, Sigma Aldrich), and 3.17 g of the di-functional thiol spacer monomer, 2,2-(ethylenedioxy) diethanethiol (EDDET, Sigma Aldrich) were added and mixed. The mixture was heated again for ca. 15 min and allowed to cool.

Indium and gallium (EASCHEM, 99.99%) were alloyed (25:75 wt. content In:Ga) by first melting gallium in a 100 °C oven and then adding indium. After alloying at elevated temperatures until no solid indium remained, the LM alloy was added to the LCE mixture in the amount of 60 vol. % LM. A small amount of toluene (< 2 g) was added and the LM was sheared into mm-sized droplets by stirring with a wooden stirrer. Multiple batches of LM-LCE composites were synthesized with different particle sizes by changing mixing parameters.

Composites with *O*(100 μm) particles were formed by mixing with a Scilogex OS20-S overhead stirrer at 1000 RPM for 60 s after mixing by hand. To investigate processing differences, a second batch of particles were mixed at 1000 RPM for 10 s after mixing by hand. To investigate any batch-to-batch variability given identical processing conditions, two batches of composites with *O*(10 μm) were mixed at 1000 RPM for 60 s, followed by mixing at 2200 RPM for > 30 s. For composites with *O*(10 μm) particles, more toluene was added as the mixture became viscous to prevent unwanted solidification. A water bath was used during mixing to keep the mixture cool. LM droplet size and size dispersity may vary between batches due to changes in viscosity during mixing as the LCE polymerizes and due to variability in initial shearing to mm-sized droplets. Further optimization could be implemented if precise size control is desired with droplet size, where droplet size and dispersity are influenced by mixing speed/time.[33] In evaluating the influence of droplet size, the order of the droplets (e.g., *O*(10 μm) vs *O*(100 μm)) has a greater effect than individual batch-to-batch variation.

Composites with *O*(1 μm) particles were synthesized by probe sonication. 5 g of LM were added to vials with 20 g of ethyl acetate and sonicated for > 10 min. Multiple batches were combined, and the ethyl acetate was evaporated. The nano-sized particles were dried and re-dispersed in the uncured LCE mixture to make the 60 vol. % LM-LCE composite.

To catalyse polymerization, 1.5 g of 1:50 dipropylamine (DPA, Sigma Aldrich):toluene were mixed into the uncured LM-LCE mixtures. The mixtures were stirred until highly viscous and poured into polyethylene moulds. The polymerization proceeded for > 5 h, and the stiff gel was placed in a 90 °C vacuum oven for > 8 h to completely remove toluene. All LCEs were polydomain

2.2 Materials characterization

Mechanical and thermomechanical characterizations were performed using a TA Instruments RSA-G2 solids analyser with a forced convection oven. Temperature-dependent dynamic mechanical analysis (DMA) of rectangular samples was used to evaluate the mechanical properties and transition temperatures. Samples were tested at 0.4 % strain and 1 Hz while heating and cooling at a rate of 3 °C min^{-1}. All samples were annealed above the transition temperature and allowed to cool to room temperature for > 24 h before testing. Temperature sweeps were dependent on sample due to limitations of the maximum force of the instrument but were heated to 120 °C before cooling. The isotropic transition temperature (T_{NI}) was associated with a minimum in the storage modulus.[5,40]

Stress-strain characteristics were evaluated at a strain rate of 50 % min^{-1} until fracture using a TA Instruments RSA-G2 solids analyser. Samples were secured with adhesive grips to prevent slipping.

Thermomechanical actuation characteristics were tested under constant stress. Samples were heated to 150 °C, were allowed to equilibrate and were subsequently heated and cooled at 5 °C min^{-1}

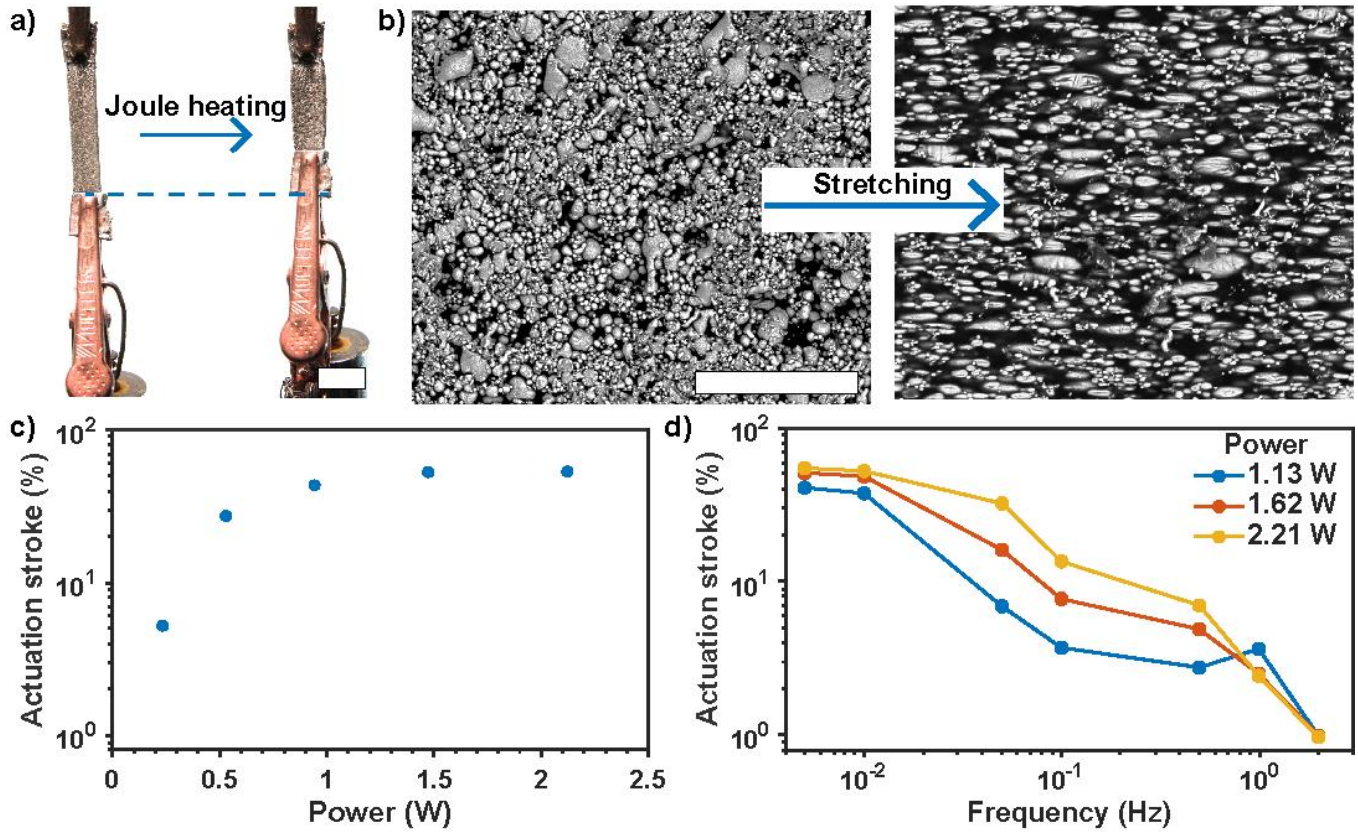

Fig. 1 (a) Photographs of a 60 vol. % LM-LCE composite lifting a weight by Joule heating. The dashed line is a guide for the eye to show the macroscopic change in shape. The scale bar is 10 mm. A video of repeated actuation is available in the ESI. (b) Micrographs of a 60 vol. % LM-LCE composite with LM particles prepared by probe sonication. The LM particles deform when stretched (right) with the stretching direction in the direction of the arrow. The scale bar is 30 µm. (c) Actuation stroke as a function of input electrical power for a 60 vol. % LM-LCE. The temperature of the soft actuator equilibrated at the input power for > 60 s, followed by cooling to room temperature. The values displayed are an average for n = 3 cycles. Standard deviations were ≤ 13% of the measured value for all input power. (d) Actuation stroke as a function of cycling frequency for three input powers at 20 % duty cycle. The values displayed are an average for n ≥ 3 cycles. Standard deviations were ≤ 15% of the measured value for all input power.

while measuring the displacement. The length of the sample in the isotropic state was defined as the average gap height between 120 °C and 140 °C and was tracked during cooling for analysis. The thermomechanical characteristics were evaluated by the ratio between the length of the sample in the isotropic state (L_{iso}) and the length of the same at the applied load in the nematic state at ca. 35 °C (L).

Thermal characteristics were also evaluated by differential scanning calorimetry (DSC) using a TA Instruments Q20 and heating and cooling from -90 °C to 50 °C at a rate of 5 °C min^{-1}.

A Quanta 200 scanning electron microscope (SEM) was used to analyse particle sizes. A back-scattered electron detector was used to improve contrast. Cross-sections were freeze fractured using liquid nitrogen. Samples were coated with 2 nm Au to prevent charging during measurement. Particle sizes were evaluated in ImageJ. Stretched composites analysed by SEM were not coated with Au and were subjected to > 100 % strain manually and affixed to the SEM sample stage.

2.3 Joule-heated actuation characterization

For Joule-heated actuation, LM-LCE composites were made electrically conductive by mechanical sintering[35], which involved applying a pressure to the composite. The electrical connection points of the composite were spray-coated with a thin layer of LM to improve the electrical connection to the leads of the Korad KA3010d precision variable adjustable power supply. The power supply was connected to the composite by copper contacts that were coated with LM by dipping in diluted hydrochloric acid and LM. Power was measured by controlling the input current and measuring the resistance of the composite using a four-point probe multimeter. The actuation properties were tracked using digital video and MATLAB, 2018a. To control duty cycle and actuation frequency, the power supply was interfaced with a microprocessor (Arduino Uno), and power was cycled using a MOSFET.

3. Results & Discussion

3.1 LM-LCE actuation characteristics

The LM-LCE soft actuator is capable of Joule-heated actuation with high stroke and actuation stress on the order of natural muscle (Fig. 1a). LM deforms with the surrounding matrix material, permitting Joule-heated actuation (Fig. 1b). The actuation stroke as a function of input power was evaluated for a 60 vol. % LM-LCE soft actuator. The composite was allowed to equilibrate at the input power for > 60 s and then cooled to room temperature while we tracked the actuation stroke. As the input power is increased, the actuation stroke increased until the stroke saturated (Fig. 1c).

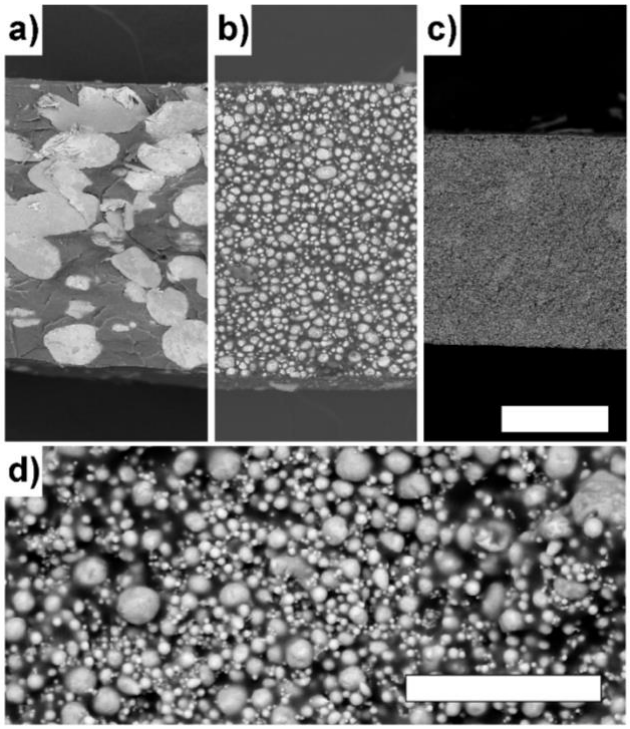

Fig. 2 Micrographs of cross-sections of 60 vol. % LM-LCE composites with *O*(100 µm) (a), *O*(10 µm) (b), and *O*(1 µm) (c) particles. The scale bar in (c) represents 250 µm and is applicable for (a)-(c). A zoomed view shows the *O*(1 µm) particles (d). The scale bar in (d) represents 20 µm.

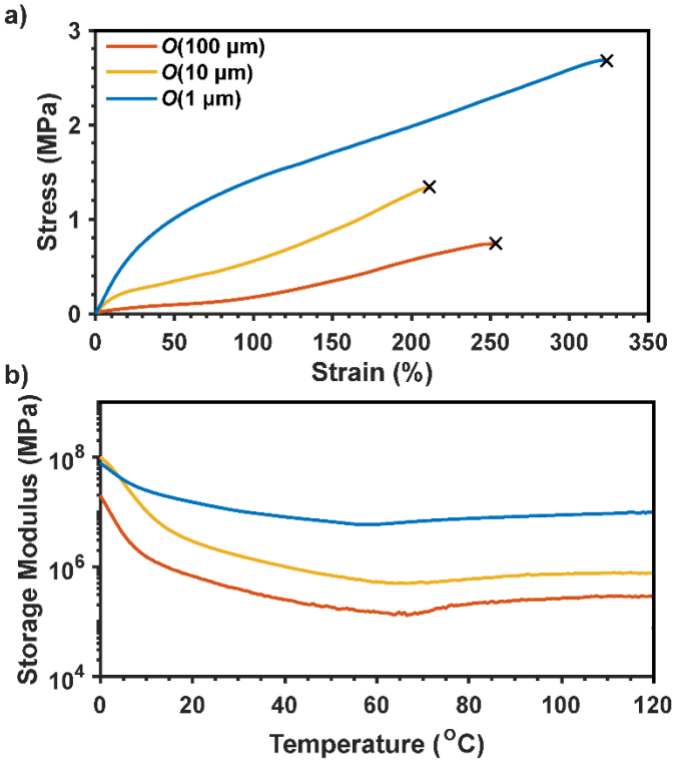

Fig. 3 (a) Representative stress-strain characteristics of LM-LCE composites with *O*(100 µm), *O*(10 µm), or *O*(1 µm) particles. (b) Storage modulus as a function of temperature as measured by DMA for LM-LCE composites with *O*(100 µm), *O*(10 µm), or *O*(1 µm) particles

The actuation stroke as a function of frequency was measured at a duty cycle of 20 % for three different input powers (Fig. 1d). The energy efficiency was also calculated by measuring the input electrical energy and the output work for one full cycle. We note that actuators that operate at high frequency never fully cool to room temperature and cycle between two elevated temperatures. We assumed the energy required to reach these elevated temperatures would be negligible for a continuously operating actuator and did not include it in our calculation of efficiency. We expected the energy efficiency to be low[3] and found a maximum efficiency of 0.05 % (Fig. S1). We also measured the dependence of actuation properties on duty cycle at 0.1 Hz and 1.62 W and found local maxima for stroke and efficiency (Fig. S1). Generally, there is a trade-off between actuation stroke and efficiency that could be balanced depending on application needs.

We note that we performed these tests using a load of about 15 kPa, which is well below the maximum stress that the LM-LCE could lift (80-90 kPa). Regardless, further improvements in efficiency are desirable and could be achieved by (i) operating in a small temperature window over which the shape change of the LCE is large, (ii) lowering the transition temperature of the LCE, or (iii) increasing the actuation stress of the composite. The ability to tune electrical, mechanical, and thermal properties of LCE soft actuators will be important for wide use as artificial muscles.

3.2 LM-LCE particle size and materials properties

One possibility to tune the properties of LM-LCE composites is to control the particle size by modifying mixing parameters. By increasing the mixing time and/or speed, particles were sheared to smaller sizes. Even smaller particles were formed by probe sonication. Particle sizes were analysed by viewing the cross-section of cured composites by electron microscopy (Fig. 2). We note that absolute particle sizes may be different than the values we report, since particles could be buried in the polymer matrix. We identify particles in this manuscript by their relative size: *O*(100 µm), *O*(10 µm), and, *O*(1 µm) (Table 1).

Two batches of composites with *O*(100 µm) particles were made, and particles were 160 ± 88 µm (Fig. S2) and 110 ± 54 µm in diameter (Fig. 2a). Two batches of composites with *O*(10 µm)

Table 1. Properties of LM-LCE composites for different particle sizes. Two batches of *O*(100 µm) and *O*(10 µm) were evaluated LM-LCE composites to investigate processing and batch-to-batch variations. Average values and standard deviations where given are shown with n ≥ 3.

Composite designation	Particle size (µm)	Elastic modulus (MPa)	Strain at break (%)	Storage modulus @ 25 °C (MPa)	L/L_{iso} @ 70 kPa	L/L_{iso} @ 250 kPa	L/L_{iso} @ 600 kPa
***O*(100 µm) LM-LCE**	160 ± 88; 110 ± 54	0.32 ± 0.10; 0.25 ± 0.06	345 ± 54; 279 ± 30	0.22; 0.49	1.61 ± 0.05 1.51 ± 0.04	-	-
***O*(10 µm) LM-LCE**	7.2 ± 5.2; 10.5 ± 6.0	0.80 ± 0.16; 1.6 ± 0.3	314 ± 41; 237 ± 86	2.0 2.1	1.046 ± 0.001; 1.069 ± 0.062	1.21 ± 0.02; 1.13 ± 0.03	-
***O*(1 µm) LM-LCE**	0.9 ± 0.8	4.3 ± 1.5	356 ± 132	12.1	≤ 1.01	≤ 1.01	1.05 ± 0.03

particles were made, and particles were 7.2 ± 5.2 µm (Fig. S2) and 10.5 ± 6.0 µm in diameter(Fig. 2b). Composites with *O*(1 µm) particles contained particles that were 0.9 ± 0.8 µm in diameter (Fig. 2c, Fig. 2d).

The particle size of liquid particles in a solid matrix can influence mechanical properties, and small liquid particles can stiffen a soft composite. Stiffening for small liquid droplets is related to an increase in total interfacial area between the matrix and liquid. This interfacial area is influenced by an imposed stress as the matrix and droplets deform.[39] To examine this stiffening, we first evaluated the stress-strain characteristics (Fig. 3A, Table 1, Fig. S3). The elastic moduli at small strain (Fig. S4) for composites with *O*(100 µm) particles (0.32 ± 0.10 MPa and 0.25 ± 0.06 MPa) were not significantly different. These moduli are similar to that of the unfilled LCE.[31] The elastic moduli increased for both batches of composites that contained *O*(10 µm) particles, up to a value of 1.6 ± 0.3 MPa for one batch. Composites with *O*(1 µm) particles had an even larger average elastic modulus of 4.3 ± 1.5 MPa. All composites were deformable with strains at break > 200 %.

A plateau in the stress-strain characteristics for the composites with *O*(100 µm) particles corresponds to so-called soft elasticity that occurs with reorientation of liquid crystal domains.[41] Notably, the regime associated with soft elasticity appears steeper for composites with *O*(10 µm) particles and is absent for composites with *O*(1 µm) particles. This observation may relate to disrupted ordering of liquid crystal domains, or it may be a consequence of the combined influence of the liquid metal/elastomer interface along with the stretching of the elastomer matrix. Further characterization (e.g., through *in-situ* X-ray scattering) could add insight into this observation.

The mechanical properties were also evaluated by temperature-dependent DMA. Samples were heated and cooled for multiple cycles (Fig S5), and representative cycles show a similar trend in the mechanical response vs. particle size as the stress-strain characteristics (Fig. 3b). Specifically, we looked at the storage modulus at 25 °C and saw that the storage modulus increased from 0. 22 MPa for composites with *O*(10 µm) particles up to 12.1 MPa for composites with *O*(1 µm) particles. Observations through DMA were consistent with stress-strain characteristics.

Temperature-dependent DMA can also capture the thermal transitions that occur in the composites. Namely, T_{NI} and the melting temperature of the LM were of interest. T_{NI} is associated with a dip in the storage modulus and was observed at similar temperatures in all composites, suggesting that particles of all size remain grossly phase separated. A shoulder peak in the tangent of the phase angle between storage and loss moduli also corresponded with T_{NI} (Fig. S6). The minimum of the storage modulus was typically between 60 and 70 °C, which was expected for the specific liquid crystal monomer that we used.[5,31,40] Composites made with *O*(1 µm)particles had a storage modulus minimum at a slightly lower temperature (58-59 °C).

LM supercooling was apparent in these composites. Bulk LM freezes at -11 °C while a spike in the storage modulus attributed to LM freezing was not observed until < -20 °C (e.g., Fig. S5).[37] Full characterization of the LM supercooling was difficult with DMA since the high-volume content of LM stiffened the composites beyond the measurement range of the instrument. Supercooling was confirmed by DSC, and composites with *O*(10 µm) or *O*(1 µm) particles had multiple melting and freezing transitions, which may be attributed to high polydispersity (Fig. S7). LM supercooling may be useful for low-temperature applications, but the LCE matrix would have to be redesigned to lower the glass transition temperature.

3.3 LM-LCE particle size and actuation properties

Importantly, the LM-LCE soft actuators should display reversible actuation under an applied load. The thermomechanical response of LM-LCE composites was monitored. LM-LCE composites with *O*(100 µm) particles retained > 50 % actuation strain upon application of a 70 kPa load (Table 1, Fig. 4). The reversible shape change increased with increasing dead load (Fig. S8). Increasing the stress broadened the transition from the isotropic to nematic state (Fig. S8). The LM-LCE composites with *O*(10 µm) and *O*(1 µm) particles had < 5 % reversible shape change upon application of a 70 kPa load. LM particle loading influenced the actuation strain and lower loadings exhibited increased reversible shape change but wouldn't be electrically conductive (Fig. S9).

When referring to the stress-strain characteristics (Fig. 3a), LM-LCE composites with *O*(10 µm) and *O*(1 µm) particles will not stretch to meaningful strains (< 5 %) under a 70 kPa load. It would follow that a larger load should induce larger actuation strain for these composites (Fig. S10). At 250 kPa, the LM-LCE composites with *O*(10 µm) particles exhibited up to 21 ± 2 % actuation strain. Note that composites with *O*(100 µm) particles typically failed at stress values < 110 kPa. LM-LCE composites with *O*(10 µm) failed at stress values between 290-350 kPa.

LM-LCE composites with *O*(1 µm) particles averaged 5 ± 3 % actuation strain at 600 kPa with actuation > 1 % not apparent until loads of 300 kPa or greater (Fig. S12). The loading gap continued to increase through repeated actuation cycles, but actuation strains at loadings ≥ 600 kPa were supported by those

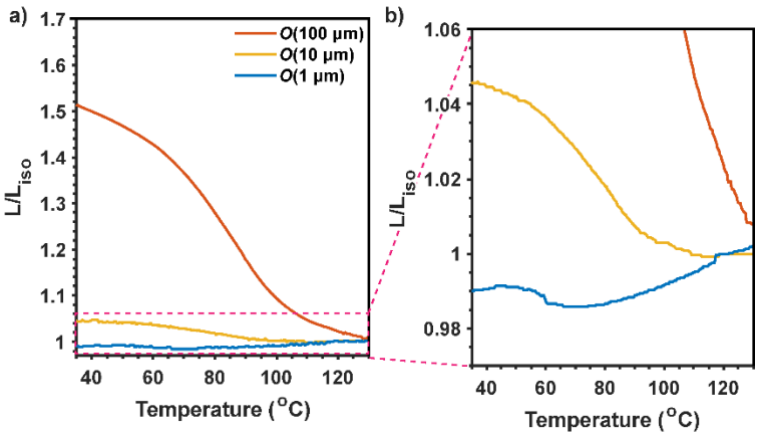

Fig. 4 (a) Representative thermomechanical actuation characteristics of LM-LCE composites with different sized particles. (b) A zoomed view of the normalized isotropic length change as a function of temperature to visualize the change in length for LM-LCE composites with O(10 µm) and O(1 µm) particles. A 70 kPa load was used for these measurements. The cooling cycles are shown.

measured by Joule heating (Fig. S12). This apparent increase in gap height with each loading cycle could be related to stress relaxation and/or a Mullin's-like effect that has been observed in many LM composites.[42] Note that some LM-LCE composites with *O*(1 µm) particles broke at ≤ 600 kPa while some could actuate with greater loads. For 8 samples, 1 failed at < 600 kPa, 3 failed at 600 kPa or were not tested at > 600 kPa, and the rest failed at > 600 kPa. In some cases, stress concentrations near the clamps may play a role in failure.

Decreased actuation strains like those observed for composites with *O*(1 µm) and *O*(10 µm) LM particles were reported when crosslinking density increased for similar LCE networks[5], and the increase of total interfacial area between the LM and the matrix could act as physical crosslinks. Under an imposed stress, the interfacial energy between the LM droplets and LCE network increases as the droplets deform. The drive to minimize the interfacial energy could reduce reversible shape-morphing capabilities. Alternatively, the presence of LM could disrupt the formation of the monodomain by physically constraining the LCE network. If the scale of the LCE domains is much greater than the confinement of mesogen ordering at the LM-matrix interface, then the LM-matrix interface would have little effect on monodomain formation. Future work could focus on deconvolution of these effects through modelling and X-ray scattering.

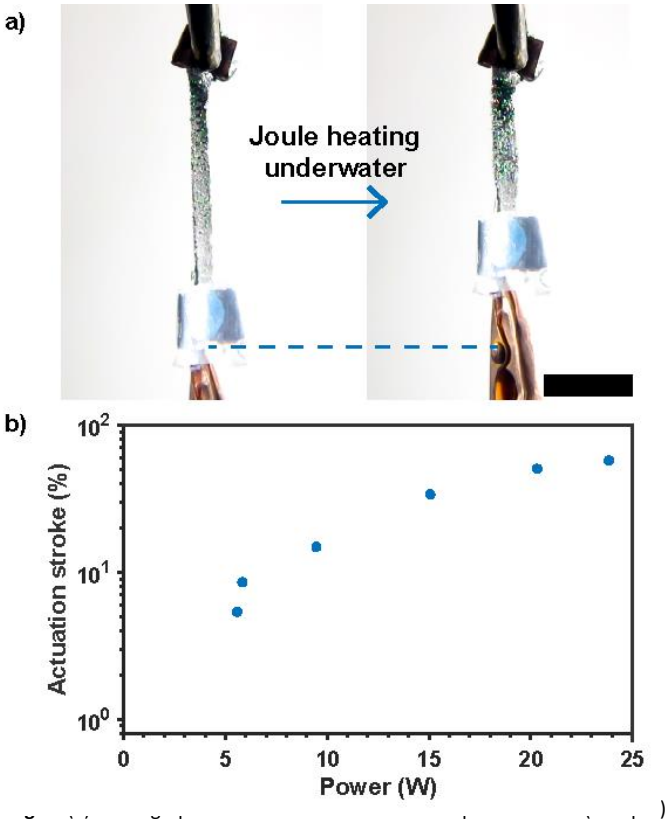

particles lifting a weight by Joule heating while underwater. The dashed line is a guide for the eye to show the macroscopic change in shape. The scale bar represents 10 mm. (b) Actuation stroke as a function of input electrical power for a 60 vol. % LM-LCE with *O*(100 µm) particles actuated underwater. The soft actuator was cycled at 0.5 Hz with a duty cycle of 50 %. The values displayed are an average for n = 3 cycles. Standard deviations were ≤ 9% of the measured value for all input power.

There is a trade-off between actuation stress and actuation strain in these composites. Some LM-LCE composites with *O*(1 µm) particles broke at ≥ 600 kPa while no LM-LCE composites with *O*(100 µm) exceeded actuation stress > 110 kPa. Concomitantly, LM-LCE composites with *O*(1 µm) particles exhibited reduced actuation stroke relative to LM-LCE composites with *O*(100 µm) particles. It should be noted that total work output may be reduced for LM-LCE composites with *O*(1 µm) particles. Still, the ability to tune actuation properties may be useful for certain applications that require higher actuation stress but lower actuation strain. This feature is analogous to shape memory alloys that are programmed into springs to increase actuation strain while sacrificing actuation stress.[43] As a demonstrative example of actuation trade-off where stress is increased, a LM-LCE actuator that contained *O*(1 µm) particles could lift ca. 900 × its mass by Joule heating (1 MPa load), a meaningful improvement relative to a previous embodiment of LM-LCE composite that could lift 193 × its mass (Video S1).[31]

Alternatively, if the desired application is high strain at moderate loads, the composites with *O*(100 µm) particles should be used. In addition, since practical implementations of the soft actuators would require faster actuation, we considered actuation in a convective fluid (i.e, water). A load (10-15 kPa) was hung from a LM-LCE composite with *O*(100 µm) particles in water (Fig. 5a). The soft actuator was Joule heated at 0.5 Hz and a 50 % duty cycle at various input electrical power (Fig. 5b, Video S2). As with actuation in air (Fig. 1c), increases in input power led to greater actuation stroke. Note that due to heat dissipation of the convective fluid, the input power necessary to reach > 50 % actuation stroke was higher than the input power in air. However, the actuation stroke was larger at high frequencies since cooling was faster in water. For example, at 2 Hz, 20.3 W, and 20 % duty cycle, the actuation strain was 15.5 ± 1 %, and the efficiency was 0.02 %, which is comparable to the soft actuator that was tested in air (Video S3, Fig. S1). The underwater soft actuator demonstrates a useful implementation of high strain actuation of these LM-LCE composites.

Conclusions

Continued development of soft actuators will rely on improvements in synthesis and processing of shape morphing materials. LM-LCE composites are promising candidates for soft actuators and may be further improved by structure-property investigations. In this work, we showed that the particle size of gallium-based LM alloys can be easily tuned by simple shear mixing or probe sonication and influences the actuation properties of related composites. In LCE composites, smaller LM particles increased the elastic modulus from 0.3 MPa to 4.3 MPa, which meant that a LM-LCE soft actuator would have meaningful differences in actuation properties at a given deadload. For LM-LCE composites made with larger particles, actuation strains > 50 % were achieved but composites typically failed when lifting between 70 and 110 kPa. For LM-LCE composite with smaller particles, actuation strains were reduced relative to composites with larger particles at similar

loads but could lift loads exceeding 600 kPa. The tunability of actuation properties unlocks a new design space for soft actuators that use these composites. Such tunability will be useful for artificial muscle applications in soft robotics, healthcare, and wearable computers among other technologies.

Conflicts of interest

There are no conflicts to declare.

Acknowledgements

The authors would like to acknowledge use of the Materials Characterization Facility at Carnegie Mellon University under grant # MCF-677785. This material is based upon work supported by, or in part by, the US Army Research Laboratory and the US Army Research Office under Contract/Grant W911NF1810150 (Program Manager: Dr. Samuel C. Stanton).

Notes and references

1 J. D. W. Madden, N. A. Vandesteeg, P. A. Anquetil, P. G. A. Madden, A. Takshi, R. Z. Pytel, S. R. Lafontaine, P. A. Wieringa and I. W. Hunter, *IEEE Journal of Oceanic Engineering*, 2004, **29**, 706–728.
2 S. M. Mirvakili and I. W. Hunter, *Advanced Materials*, 2018, **30**, 1704407.
3 J. E. Huber, N. A. Fleck and M. F. Ashby, *Proceedings of the Royal Society of London. Series A: Mathematical, Physical and Engineering Sciences*, 1997, **453**, 2185–2205.
4 H.-F. Lu, M. Wang, X.-M. Chen, B.-P. Lin and H. Yang, *J. Am. Chem. Soc.*, 2019, **141**, 14364–14369.
5 M. O. Saed, A. H. Torbati, C. A. Starr, R. Visvanathan, N. A. Clark and C. M. Yakacki, *Journal of Polymer Science Part B: Polymer Physics*, 2017, **55**, 157–168.
6 M. O. Saed, C. P. Ambulo, H. Kim, R. De, V. Raval, K. Searles, D. A. Siddiqui, J. M. O. Cue, M. C. Stefan, M. R. Shankar and T. H. Ware, *Advanced Functional Materials*, 2019, **29**, 1806412.
7 A. Kotikian, C. McMahan, E. C. Davidson, J. M. Muhammad, R. D. Weeks, C. Daraio and J. A. Lewis, *Science Robotics*, , DOI:10.1126/scirobotics.aax7044.
8 M. O. Saed, A. Gablier and E. M. Terentejv, *Advanced Functional Materials*, 2020, **30**, 1906458.
9 E. C. Davidson, A. Kotikian, S. Li, J. Aizenberg and J. A. Lewis, *Advanced Materials*, 2020, **32**, 1905682.
10 H. Wermter and H. Finkelmann, *e-Polymers*, , DOI:10.1515/epoly.2001.1.1.111.
11 C. P. Ambulo, J. J. Burroughs, J. M. Boothby, H. Kim, M. R. Shankar and T. H. Ware, *ACS Applied Materials & Interfaces*, 2017, **9**, 37332–37339.
12 M. López-Valdeolivas, D. Liu, D. J. Broer and C. Sánchez-Somolinos, *Macromolecular Rapid Communications*, 2018, **39**, 1700710.
13 A. Kotikian, R. L. Truby, J. W. Boley, T. J. White and J. A. Lewis, *Advanced Materials*, 2018, **30**, 1706164.
14 S. V. Ahir, A. R. Tajbakhsh and E. M. Terentjev, *Advanced Functional Materials*, 2006, **16**, 556–560.
15 S. W. Ula, N. A. Traugutt, R. H. Volpe, R. R. Patel, K. Yu and C. M. Yakacki, *Liquid Crystals Reviews*, 2018, **6**, 78–107.
16 T. J. White, N. V. Tabiryan, S. V. Serak, U. A. Hrozhyk, V. P. Tondiglia, H. Koerner, R. A. Vaia and T. J. Bunning, *Soft Matter*, 2008, **4**, 1796–1798.
17 S. Serak, N. Tabiryan, R. Vergara, T. J. White, R. A. Vaia and T. J. Bunning, *Soft Matter*, 2010, **6**, 779–783.
18 M. Camacho-Lopez, H. Finkelmann, P. Palffy-Muhoray and M. Shelley, *Nature Materials*, 2004, **3**, 307–310.
19 M. Rogóż, K. Dradrach, C. Xuan and P. Wasylczyk, *Macromolecular Rapid Communications*, 2019, **40**, 1900279.
20 H. Zeng, P. Wasylczyk, C. Parmeggiani, D. Martella, M. Burresi and D. S. Wiersma, *Advanced Materials*, 2015, **27**, 3883–3887.
21 T. Guin, B. A. Kowalski, R. Rao, A. D. Auguste, C. A. Grabowski, P. F. Lloyd, V. P. Tondiglia, B. Maruyama, R. A. Vaia and T. J. White, *ACS Appl. Mater. Interfaces*, 2018, **10**, 1187–1194.
22 S. Courty, J. Mine, A. R. Tajbakhsh and E. M. Terentjev, *Europhysics Letters (EPL)*, 2003, **64**, 654–660.
23 M. Shahinpoor, in *Smart Structures and Materials 2000: Electroactive Polymer Actuators and Devices (EAPAD)*, International Society for Optics and Photonics, 2000, vol. 3987, pp. 187–193.
24 H. Finkelmann and M. Shahinpoor, in *Smart Structures and Materials 2002: Electroactive Polymer Actuators and Devices (EAPAD)*, International Society for Optics and Photonics, 2002, vol. 4695, pp. 459–465.
25 D. L. T. Iii, G. Bush, P. Keller and R. G. Bryant, in *Smart Structures and Materials 2002: Electroactive Polymer Actuators and Devices (EAPAD)*, International Society for Optics and Photonics, 2002, vol. 4695, pp. 435–441.
26 C. M. Spillmann, J. Naciri, B. D. Martin, W. Farahat, H. Herr and B. R. Ratna, *Sensors and Actuators A: Physical*, 2007, **133**, 500–505.
27 Y. Y. Huang, J. Biggins, Y. Ji and E. M. Terentjev, *Journal of Applied Physics*, 2010, **107**, 083515.
28 S. Petsch, R. Rix, B. Khatri, S. Schuhladen, P. Müller, R. Zentel and H. Zappe, *Sensors and Actuators A: Physical*, 2015, **231**, 44–51.
29 Y.-Y. Xiao, Z.-C. Jiang, X. Tong and Y. Zhao, *Advanced Materials*, 2019, **31**, 1903452.
30 Q. He, Z. Wang, Y. Wang, A. Minori, M. T. Tolley and S. Cai, *Science Advances*, 2019, **5**, eaax5746.
31 M. J. Ford, C. P. Ambulo, T. A. Kent, E. J. Markvicka, C. Pan, J. Malen, T. H. Ware and C. Majidi, *PNAS*, 2019, **116**, 21438–21444.
32 M. D. Dickey, *Advanced Materials*, 2017, **29**, 1606425.
33 I. D. Tevis, L. B. Newcomb and M. Thuo, *Langmuir*, 2014, **30**, 14308–14313.
34 J. N. Hohman, M. Kim, G. A. Wadsworth, H. R. Bednar, J. Jiang, M. A. LeThai and P. S. Weiss, *Nano Letters*, 2011, **11**, 5104–5110.
35 J. W. Boley, E. L. White and R. K. Kramer, *Advanced Materials*, 2015, **27**, 2355–2360.
36 C. Pan, E. J. Markvicka, M. H. Malakooti, J. Yan, L. Hu, K. Matyjaszewski and C. Majidi, *Advanced Materials*, 2019, **31**, 1900663.
37 M. H. Malakooti, N. Kazem, J. Yan, C. Pan, E. J. Markvicka, K. Matyjaszewski and C. Majidi, *Advanced Functional Materials*, 2019, **29**, 1906098.
38 Z. H. Han, B. Yang, Y. Qi and J. Cumings, *Ultrasonics*, 2011, **51**, 485–488.
39 R. W. Style, R. Boltyanskiy, B. Allen, K. E. Jensen, H. P. Foote, J. S. Wettlaufer and E. R. Dufresne, *Nature Physics*, 2015, **11**, 82–87.

40 C. M. Yakacki, M. Saed, D. P. Nair, T. Gong, S. M. Reed and C. N. Bowman, *RSC Adv.*, 2015, **5**, 18997–19001.
41 M. Warner, P. Bladon, E. Terentjev, *J. Phys. II France*, 1994, **1**, 93-102.
42 L. Mullins, *Rubber Chem. Technol.* 1969, **42**, 339-362.
43 J. Mohd Jani, M. Leary, A. Subic and M. A. Gibson, *Materials & Design (1980-2015)*, 2014, **56**, 1078–1113.

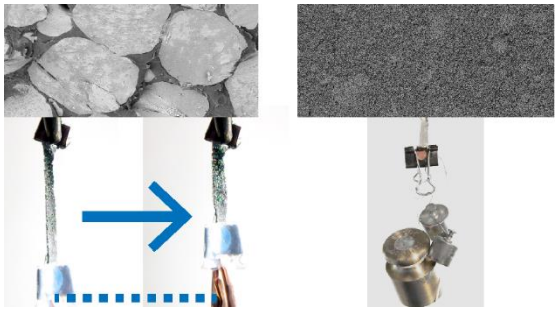

A shape-morphing composite exhibits tunable actuation properties (stroke and force output) that are influenced by liquid metal particle size.